PAPER

Electrical transport properties of microwave-synthesized $Bi_2Se_{3-x}Te_x$ nanosheet†

Haiming Xu, Gang Chen,* Rencheng Jin, Dahong Chen, Jian Pei and Yu Wang

Tellurium (Te) doped bismuth selenide ($Bi_2Se_{3-x}Te_x$) nanosheets have been successfully synthesized by the microwave-assisted method in the presence of ethylene glycol (EG). The obtained products were characterized by powder X-ray diffraction (XRD), field-emission scanning electron microscopy (FESEM), transmission electron microscopy (TEM), high-resolution TEM (HRTEM), selected-area electron diffraction (SAED), X-ray photoelectron spectroscopy (XPS) and Raman spectroscopy techniques. The electrical transport properties of the nanosheets are investigated by measuring the electrical conductivity and the Seebeck coefficient at temperatures ranging from 298 to 523 K. The power factor values of the $Bi_2Se_{3-x}Te_x$ nanosheet vary with different doping concentrations of Te, and the maximum power factor can reach 178 $\mu W\ m^{-1}\ K^{-2}$ at 523 K for $Bi_2Se_{2.7}Te_{0.3}$, indicating the potential application in thermoelectric devices.

Introduction

Thermoelectric (TE) materials are considered as critical components for solid state thermoelectric cooling and electrical power generation devices.[1,2] These thermoelectric (TE) devices have a wide variety of applications from cooling devices for seats in luxury automobiles to power supplies for spacecraft. Compared with other refrigeration or electric power generation, this kind of device demonstrates many attractive features such as long life, no moving parts, no emission of toxic gases, low maintenance and high reliability.[3,4] Thus, a broad and intense search has been devoted to identify new materials with enhanced thermoelectric properties.[5–8] Nevertheless, the efficiency of the bulk thermoelectric material is extremely low as a refrigerating material when compared to the Freon-based conventional refrigerating material, which limits the practical application of TE material as a power generator and/or refrigerator.[9]

The efficiency of TE material can be defined by the dimensionless thermoelectric figure of merit ZT = $S^2\sigma T/(\kappa_e + \kappa_l)$, where S is the thermopower, σ is the electrical conductivity, κ is the thermal conductivity (κ_e and κ_l are the electronic and the lattice contributions, respectively) and T is absolute temperature at which the figure of merit is measured.[10] The quantity $S^2\sigma$ is most commonly referred to as the power factor. An ideal thermoelectric material in principle should be electrically short-circuited and thermally open-circuited with a high thermoelectric power. However, the interdependency of

Department of Chemistry, Harbin Institute of Technology, Harbin 150001, P. R. China. E-mail: gchen@hit.edu.cn; Fax: +86-451-86413753; Tel: +86-0451-86413753
† Electronic supplementary information (ESI) available: EDS of the as-prepared samples, properties and FESEM images of pure Bi_2Se_3 at different conditions. See DOI: 10.1039/c3ce40296g

the three physical parameters (S, σ and κ) imposes a limitation on the efficiency of thermoelectric materials.[1,11] In order to improve the figure of merit, one must think of ways to increase the value of $S^2\sigma$ and decrease the thermal conductivity. Since these properties are determined by the details of electronic structure (band gap, band shape, band degeneracy near the Fermi level) and scattering of charge carriers, they are not independent of each other.[3] Currently, the improvement of ZT is mostly driven in two directions: (i) to improve the performance of the material by doping[11,12] and synthesis methods[13,14] and (ii) to develop a module or device.[15,16]

Bismuth selenide, a V–VI semiconductor with a band gap of ~0.3 eV, belongs to a class of narrow band gap layered semiconductors with tetradymite structure.[17–20] Due to the existing six valley degeneracy and the narrow energy gap, Bi_2Se_3 is attractive for good electrical conduction, meanwhile its layered crystal structure leads to a poor thermal conductivity, making these layered materials suitable for thermoelectric applications.[21] Recently, Chen's group have fabricated the Bi_2Ch_3 films (Ch = S, Se) with high crystallinity and excellent TE performance by rational design of the precursor at low temperature (~70 °C).[22–25] However, this research has not significantly improved the properties of Bi_2Se_3. Therefore, more and more studies have been performed on the effect of doping on the bismuth selenide material. Lošťák *et al.* demonstrated that doping with certain impurities could enhance the electrical transport properties and appear even a range of unusual properties.[26–28] For example, doping Bi_2Se_3 by some IIIA elements such as In or Tl increases the power factor as much as 25%.[26–28] Furthermore, according to Kašparová,[29] a crossover of the Seebeck coefficient sign occurs for Bi_2Se_3 material by incorporation of Pb at a high level. Shokr *et al.* also reported the power factor (13.53 $\mu W\ K^{-2}\ cm^{-1}$) of

Table 1 Precursor-ratio and synthesis conditions of the $Bi_2Se_{3-x}Te_x$ (as named) nanosheet

Sample (precursor-ratio)	Synthesis conditions
Bi_2Se_3	0.1297 g Na_2SeO_3 + 0.2424 g $Bi(NO_3)_3 \cdot 5H_2O$ + 50 ml EG + 1 g KOH
$Bi_2Se_{2.9}Te_{0.1}$	0.1254 g Na_2SeO_3 + 0.0055 g Na_2TeO_3 + 0.2424 g $Bi(NO_3)_3 \cdot 5H_2O$ + 50 ml EG + 1 g KOH
$Bi_2Se_{2.7}Te_{0.3}$	0.1167 g Na_2SeO_3 + 0.0166g Na_2TeO_3 + 0.2424 g $Bi(NO_3)_3 \cdot 5H_2O$ + 50 ml EG + 1 g KOH
$Bi_2Se_{2.5}Te_{0.5}$	0.1081 g Na_2SeO_3 + 0.0277 g Na_2TeO_3 +0.2424 g $Bi(NO_3)_3 \cdot 5H_2O$ + 50 ml EG + 1 g KOH

Bi_2Se_3 was significantly improved due to doped Sb.[30] Saji[31] and George[32] have reported the growth, morphology, hardness and thermal diffusivity of Bi_2Se_3 single crystals and the effects of Te doping on these properties. Other than that, few studies involve how the electrical transport properties change due to doping with Te. Hence we tried to introduce foreign atoms to improve the performance of Bi_2Se_3 and also compared the electrical transport properties of Bi_2Se_3 crystals after doping.

Experimental section

Materials and synthesis procedures

All chemicals were analytical grade and used without further purification. Bi_2Se_3 and $Bi_2Se_{3-x}Te_x$ nanosheets were synthesized using a microwave-assisted method in ethylene glycol (EG). In a typical synthesis, a stoichiometric ratio of bismuth nitrate ($Bi(NO_3)_3 \cdot 5H_2O$), sodium selenide (Na_2SeO_3), sodium tellurite (Na_2TeO_3) and potassium hydroxide (KOH) were dissolved in 45 ml ethylene glycol in 100 mL flasks at room temperature. The precursor ratio is shown in Table 1. After vigorous stirring for 5 min, 5 ml 0.1 mol L^{-1} (0.5 mmol) fresh bismuth nitrate ($Bi(NO_3)_3 \cdot 5H_2O$) of ethylene glycol solution was added into the flasks. Here the solvent EG also works as a reducing agent for the elemental species. Then, the mixture was microwave-heated to 180 °C for 25 min. After cooling to room temperature, the product was separated by centrifugation, washed with deionized water and absolute ethanol several times, and then dried at 60 °C in a vacuum overnight. The microwave oven used was a focused multi-mode microwave synthesis system (2.45 GHz, maximum 1000 W, MAS-II, Sineo, China), which was equipped with magnetic stirring and a water-cooled condenser. Temperature was controlled by automatic adjustment of the microwave power.

Characterization

XRD patterns were recorded over the 2θ range from 10° to 90° at a speed of 10° min^{-1} using a Rigaku D/max-2000 device equipped with Cu Kα radiation (λ = 0.15406 nm). Field-emission scanning electron microscopy (FESEM, FEI, Quanta 200F) and transmission electron microscopy (TEM, FEI, Tecnai G2 S-Twin) were employed to observe the morphology of the samples. X-ray photoelectron spectroscopy (XPS) measurements were performed on a PHI 5700 ESCA System with an excitation source of Al Kα = 1486.6 eV. Raman spectroscopy was recorded (Horiba Jobin Yvon CO. Ltd) using a 632.8 nm laser with an incident power of 0.5 mW.

Thermoelectric transport measurement

To measure the electrical conductivity and Seebeck coefficient of the as-prepared samples, the bar-shaped samples (10 × 4.6 × 0.5 mm^3) were prepared under 20 MPa pressure at room temperature. Then, the sample was sintered for 6 seconds in a microwave oven (G80F23CSL-X2(G0), Galanz, China) under vacuum conditions. Silver paste electrodes coated on the specimen were used as electrical contacts. The four-probe technique was employed for the electrical conductivity measurement. For the measurement of the Seebeck coefficient, a microheater was applied to create a temperature difference (about 3–15 K) between the cool and hot ends of the specimen. A temperature gradient was established in the samples when the electrical power was applied by a thermoelectric pile. Two thermocouples were contacted to the surface of the sample to detect the temperature drop (ΔT), while the resulting thermally induced voltage ΔV was tested by the voltage probes. Then the Seebeck coefficient can be obtained by the formula, $S = -\Delta V/\Delta T$. The data of electrical conductivity and Seebeck coefficient were collected by a computer-controlled multifunctional measuring system with a flow of argon 1 mL min^{-1} (Keithley 2400 source meter, Keithley 2700 multimeter, Keithley Instruments Inc., USA).

Results and discussion

Characterization of $Bi_2Se_{3-x}Te_x$ nanosheet

The phase purity and crystal structure of the samples have been identified by X-ray diffraction and the spectra are shown in Fig. 1a. In this pattern, all of the diffraction peaks can be steadily indexed to a rhombohedra crystal geometry of Bi_2Se_3 (JCPDS: 33-0214), no detectable impurities of Bi_2Te_3 or other phases are observed. This result demonstrated that
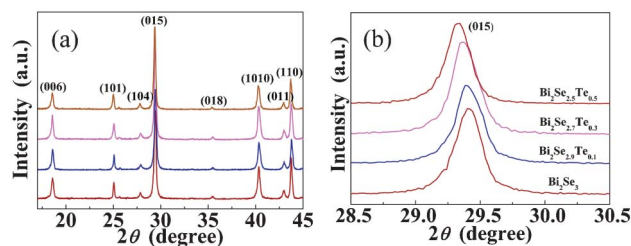
**Fig. 1** (a) XRD patterns of Bi_2Se_3 and $Bi_2Se_{3-x}Te_x$ (as named), (b) expanded view showing a systematic shift of the (015) peak for $Bi_2Se_{3-x}Te_x$ (at 28.5° to 30.5°).
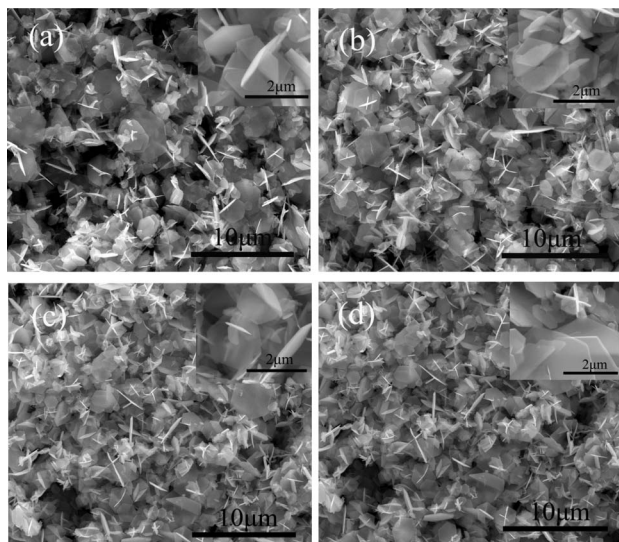
Fig. 2 FESEM images of nanosheets dispersed on a Si substrate: (a) Bi_2Se_3, (b) $Bi_2Se_{2.9}Te_{0.1}$, (c) $Bi_2Se_{2.7}Te_{0.3}$, (d) $Bi_2Se_{2.5}Te_{0.5}$.

$Bi_2Se_{3-x}Te_x$ nanosheets were successfully fabricated in the facile microwave treatment. Here, a systematic shift of the most intense XRD peaks for the 015 planes has been observed in Fig. 1b. Shift of the XRD peaks for the $Bi_2Se_{2.9}Te_{0.1}$, $Bi_2Se_{2.7}Te_{0.3}$, and $Bi_2Se_{2.5}Te_{0.5}$ may be ascribed to the doped tellurium that distorted the interface spacing of the Bi_2Se_3 crystal. The result suggests that Te have been doped into the crystal structures.[10] George[32] has reported that the lattice spacing varies from 4.134 Å for an undoped sample to 4.166 Å (for 6% of Te). Such a rapid variation in lattice spacing with the doping concentration also has been reported for II–VI doped semiconductors such as CdTe.[33] This variation in lattice spacing may be attributed to native defects in the crystals. When Bi_2Se_3 is doped with substitutional Te atoms, the lattice may distort because Se is replaced with Te of relatively larger atomic dimensions.[32] Interestingly, an obvious color change can be observed during the reaction process. In the initial stage, the mixture rapidly changed from colourless to dark at 180 °C. This change suggests that $Bi_2Se_{3-x}Te_x$ has been prepared.

To investigate the exact composition of $Bi_2Se_{3-x}Te_x$, energy dispersive spectroscopy (EDS) was used. Table S1, ESI,† gives the average value of actual (calculated) atomic wt% with experimentally observed atomic wt% from the middle portion of the crystal.

The morphology of the as-prepared products was examined by the field emission scanning electron microscopy (FESEM) technique. The corresponding SEM images were displayed in Fig. 2. It suggests that the morphology of the products is sheet with a diameter up to ~5 μm. The magnified SEM image (inset) reveals that these well-defined hexagonal nanosheets are smooth and the thickness ranges from 50 nm to 100 nm.

In order to characterize the as-prepared $Bi_2Se_{2.7}Te_{0.3}$ nanosheet, X-ray photoelectron spectroscopy (XPS) technique was used. The carbon 1 s peak was observed at the binding energy 291.3 eV, as shown in Fig. 3a. This peak was usually
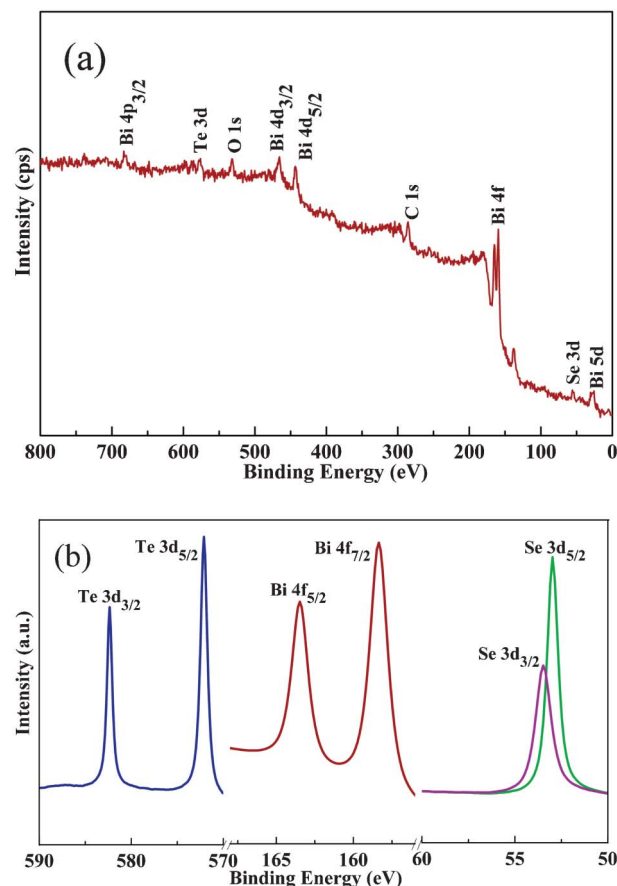

Fig. 3 XPS spectra of the $Bi_2Se_{2.7}Te_{0.3}$ nanosheets: (a) survey spectra; (b) high-resolution spectra of Te 3d, Bi 4f and Se 3d.

observed in the XPS measurements when the sample surface was exposed to the atmosphere, which was attributed to surface contamination.[34] A high-resolution scan of the Bi 4f region (Fig. 3b) shows peaks at about 158.3 and 163.4 eV, which correspond to the reported values for the binding energies of Bi $4f_{5/2}$ and Bi $4f_{7/2}$, respectively.[35] The Se 3d spectrum is broad and highly asymmetric, which can be deconvoluted into two peaks, one with a binding energy of 52.9 eV (corresponding to Se $3d_{5/2}$) and the other with 53.5 eV (corresponding to Se $3d_{3/2}$).[36] The two peaks at 572.1 and 582.4 eV can be attributed to Te $3d_{5/2}$ and Te $3d_{3/2}$, respectively, which agree well with the reported literature.[37] In addition, no peaks of other elements are observed in the wide XPS survey spectrum (Fig. 3a). These results agree well with the XRD analysis and suggest that the Te doped Bi_2Se_3 can be successfully synthesized.

Recently, Raman spectroscopy was mainly used to study the vibrational properties and electron–phonon coupling in layered compounds. We performed Raman spectroscopy measurements here to investigate how the Raman shift changes due to the tellurium doping which affected the lattice structure. The Raman spectrum of the $Bi_2Se_{3-x}Te_x$ compounds with different Te contents in the wavenumber range 80–600 cm^{-1} at room temperature are shown in Fig. 4a. There are two characteristic peaks at 132 cm^{-1} and 173 cm^{-1} within the
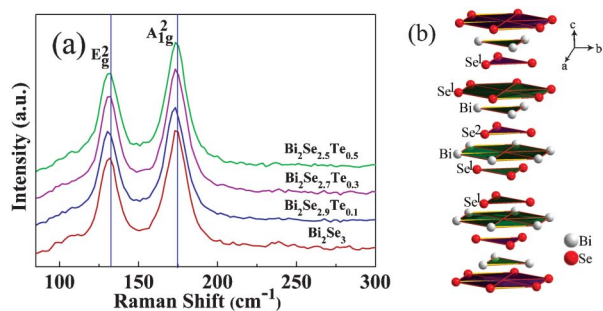
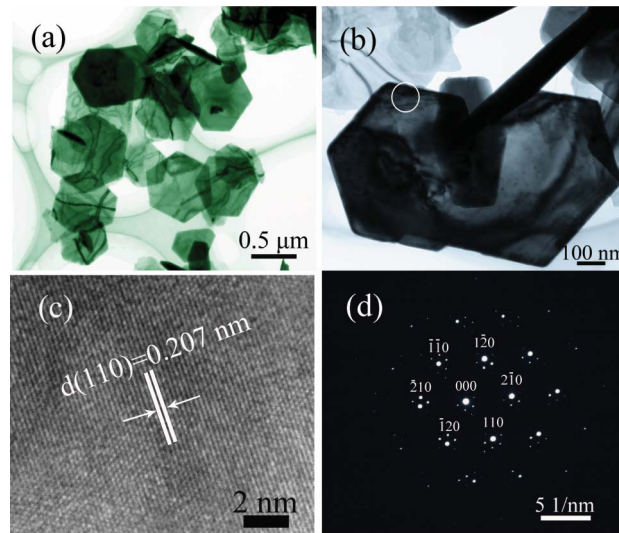**Fig. 4** (a) Raman spectrum of pure and doped $Bi_2Se_{3-x}Te_x$ nanosheets, Raman spectrum on individual nanosheets were recorded in the range of 80–600 cm^{-1}; however, for clarity, Raman shifts are shown for 80–300 cm^{-1}, (b) crystal structure of rhombohedra Bi_2Se_3.

Fig. 5 The structure and morphology of a typical $Bi_2Se_{2.7}Te_{0.3}$ nanosheet: (a) low magnification TEM image, (b) high magnification TEM image, (c) HRTEM image recorded for an individual nanosheet, (d) SAED pattern (along [001] zone axes) of the area indicated by the white circle in (b).

scanned frequency range. From the Raman selection rules given in the previous literature,[38] it follows that the peak at 132 cm^{-1} is assigned to the E_g^2 mode, and another peak (173 cm^{-1}) corresponds to A_{1g}^2 mode, which are agreement well with the previously reported experimental and calculated phonon vibration modes of Bi_2Se_3.[39–41]

The Raman shifts of the various vibrational modes with Te(x) can be observed in Fig. 4a. As is well known, layered Bi_2Se_3 has a rhombohedral crystal structure with the space group of $R\bar{3}m/D_{3d}^5$, and is composed of hexagonal close-packed atomic layers periodically arranged along the c axis. The atomic arrangement (Fig. 4b) can be considered as repeating units with each consisting of five atomic Se^1–Bi–Se^2–Bi–Se^1 layers called quintuple layers, weakly bound by van der Waals forces with a slightly covalent nature.[42,43] Therefore, Se atoms exhibit two different chemical environments (assigned as Se^1 and Se^2; Fig. 4b).[44–47] The chemical bonding between Bi–Se^2 is of a pure covalent nature, while it is slightly ionic but still covalent in nature between Bi–Se^1.[48–50] For the $Bi_2Se_{3-x}Te_x$ compounds, Te atoms will preferentially replace Se at Se^2 sites (if the replacement dosage is larger, Te will randomly replace the Se at Se^1 sites) due to Te atoms at Se^2 sites being more stable than Se^1 and thus resulting in a measurable increase in the values of the lattice parameters of $Bi_2Se_{3-x}Te_x$.[51] Therefore, the crystalline structures and lattice dynamics of Bi_2Se_3 will be changed, and eventually lead to the high frequency modes A_{1g}^2 and E_g^2 having slight Raman shifts. Soni et al. also observed Raman shifts of bismuth telluride ($Bi_2Te_{3-x}Se_x$) nanoplatelet and they attribute this phenomenon to the center mass being changed due to Se occupying the Te(2) site.[52] In addition, the dopant incorporation induced Raman spectrum broadening and weakening due to the decreasing of phonon correlation lengths caused by substitutional defects.[53,54]

In order to further investigate the microstructure of the nanosheet, TEM, HRTEM and SAED measurements were carried out. The TEM images (Fig. 5a and b) clearly reveal that the as-prepared $Bi_2Se_{2.7}Te_{0.3}$ sample is a well-defined nanosheet, which agreed well with the SEM observation. The HRTEM image of the $Bi_2Se_{2.7}Te_{0.3}$ is shown in Fig. 5c. The lattice fringe clearly revealed the presence of the (110) plane with a lattice spacing of 0.207 nm. The selected area electron

diffraction (SAED) pattern of $Bi_2Se_{2.7}Te_{0.3}$ nanosheet is presented in Fig. 5d, which indicates the single crystalline nature of the $Bi_2Se_{2.7}Te_{0.3}$ nanosheet. The bright diffraction spots in the SAED pattern can be indexed to the {110}, {$\bar{1}\bar{1}0$}, {$1\bar{2}0$}, {$\bar{1}20$}, {$\bar{2}10$} and {$2\bar{1}0$} planes of the rhombohedra $Bi_2Se_{2.7}Te_{0.3}$. In addition, it was observed that regular satellite spots appeared around the bright spots due to double diffraction. Ye et al. has reported that doping could produce lattice distortion and cause the domain structure to deviate from the ideal structure, which eventually leads to double diffraction.[55,56] In our system, the crystal structure of Bi_2Se_3 changes caused by Te replacing Se at the Se^2 sites,[57] and thus induces lattice distortion at the same time, in good agreement with the Raman analysis. According to the above TEM, HRTEM and SAED results, the single crystalline $Bi_2Se_{2.7}Te_{0.3}$ nanosheet can be successfully synthesized at 180 °C in the presence of microwave heating.

Electrical transportation properties

In order to evaluate the electrical transport property of the obtained $Bi_2Se_{3-x}Te_x$ nanosheets, the samples were first pressed into a bar with a rectangular shape of about 10 × 4.6 × 0.5 mm^3.

Bars of $Bi_2Se_{3-x}Te_x$ nanoplatelets appear with a density of 5.80 g cm^{-3} (85% of theoretical density) under the conditions specified in the Experimental section. To achieve larger densities towards 100% of the theoretical value, significantly higher microwave and duration are required, which resulted in unwanted grain growth during compaction and reduced the electrical conductivities of the samples.[11] Thus, the as-prepared bars were directly sintered in a microwave oven with vacuum conditions. The SEM technique was used to characterize the sample variation (surfaces and fractured surfaces) before and after sintering (Fig. S1 and S2, ESI†) for the sake of

studying the microwave sintering and/or pressure effect on the morphology and properties of the synthesized samples (pure Bi_2Se_3 as the model to facilitate the study). The micro-morphology of the samples is still preserved after microwave sintered and/or pressurized, suggesting that these treatments have little impact on the morphology of the as-prepared samples. Furthermore, the un-sintered samples are looser than the sintered samples. This phenomenon is mainly due to the fact that sintering can enhance the density of samples and decrease the electron transfer resistance, and thus result in the power factor of the sintered samples being higher than the un-sintered ones.[58] By analyzing the measurement results (Table S2, ESI†), the highest power factor can be obtained under 20 Mpa pressure and 6 s sintering time, thus we used this as the optimum conditions in the follow-up performance testing.

The electrical conductivities (the schematic diagram of the electrical measurement system is given in Fig. S3, ESI†) have been investigated at temperatures ranging from room temperature to 523 K (Fig. 6a) using the four probes technique. The measured electrical conductivities for the obtained products increase with increasing temperature (Fig. 6a), indicating the typical electrical conductivity of the semiconductor for the entire measuring temperature range. The measured electrical conductivity for the Bi_2Se_3 sample is 500 S m^{-1}, which is much lower than the doping tellurium samples (about 3×10^3 S m^{-1}). The increase of the electrical conductivity can be attributed to two reasons. On the one hand, the contribution of the carriers excited by the temperature change must be considered. The excitation of the carriers from the valence band to the conduction band becomes easier as the temperature increases, thus more carriers will be involved in conductivity, resulting in an increase in the electrical conductivity.[59] On the other hand, doping foreign atoms leads to an increase in the electrical conductivity. This phenomenon has been reported by Han *et al.* and Lee *et al.* in Sb_2Se_3 nanowires.[60,61] They demonstrate that surface sulfur induced donor states close to the conduction band edge and offset the low conductivity expected due to band gap broadening arising from sulfur incorporation in the sample crystal lattice, leading to a higher charge carrier mobility rather than a carrier concentration, and thus obtained higher electrical conductivity in the nanocrystals.[62]

Fig. 6b presents the temperature dependence Seebeck coefficient of the $Bi_2Se_{3-x}Te_x$ nanosheet. From this image, one can see that the Seebeck coefficient of Bi_2Se_3 and $Bi_2Se_{2.9}Te_{0.1}$ and $Bi_2Se_{2.7}Te_{0.3}$ and $Bi_2Se_{2.5}Te_{0.5}$ are negative, indicating that all the as-prepared are n-type semiconductors. All of the absolute Seebeck coefficients of the samples are increased before 473 K, then decrease. There is no reasonable explanation in literature. We proposed that after this temperature, the main carrier type of the material may change, which will lead to absolute Seebeck coefficient decreasing. The Bi_2Se_3 sample gets a maximum value 151 μV K^{-1} at 473 K, close to the value reported in the literature.[9] The Seebeck coefficient (S) of n-type Bi_2Se_3 is approximately given by the equation

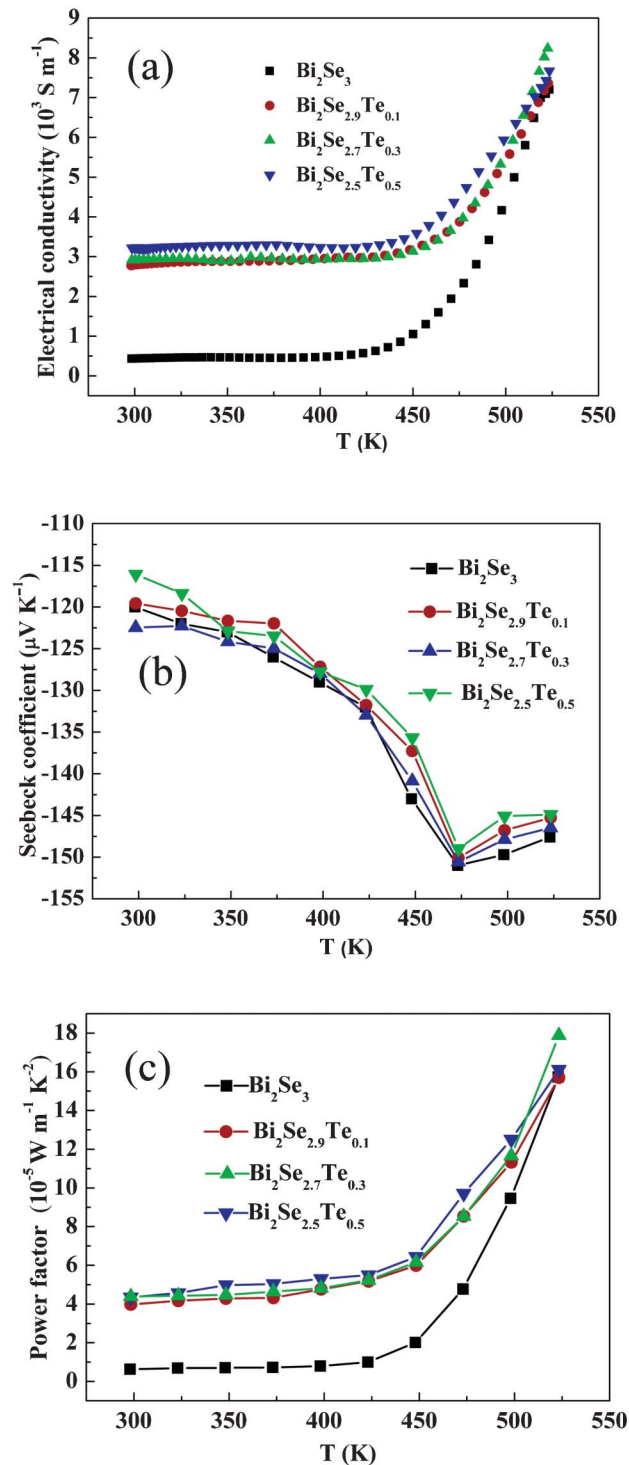$$S = BT \left(\pi/3n\right)^{2/3} \tag{1}$$

Fig. 6 Temperature dependence of thermoelectric properties of the prepared samples: (a) electrical conductivity, (b) Seebeck coefficient, (c) power factor.

where S is the Seebeck coefficient, T is the absolute temperature, n is the carrier concentration and B is the carrier effective mass (approximately constant).[63] For the present system, enhanced electrical conductivity results mainly from an increase in the carrier concentration due to temperature rather than doped tellurium. Therefore the Seebeck coefficient

will decrease as the electrical conductivity increases, which is consistent with the literature reports.[3,64]

The corresponding power factor of the samples displayed in Fig. 6c shows the dependence of the power factor on temperature. The power factor of undoped sample at room temperature is 0.62×10^{-5} W m^{-1} K^{-2}, far less than the doped samples (about 4×10^{-5} W m^{-1} K^{-2}). For the sample with x_{Te} = 0.3, values of 4.4×10^{-5} W m^{-1} K^{-2} at 298 K and 17.8×10^{-5} W m^{-1} K^{-2} at 523 K can be obtained. These values are much larger than the pure Bi_2Se_3 nanosheets and the literature report ($Bi_2Se_{2.7}Te_{0.3}$, 12.8×10^{-5} W m^{-1} K^{-2}).[3] George's group has reported that the thermal diffusivities of the doped samples are less than that of the undoped sample.[32] The reduction in the thermal diffusivity of the doped samples compared to undoped samples can be attributed to the phonon assisted heat transfer mechanism in the crystals. Phonons in the lattice suffer various additional scattering processes on the introduction of dopant. Introduction of dopants into a lattice generates extra scattering centers for phonons. These result in the reduction of the phonon mean free path. It is known that the lattice thermal conductivity (diffusivity) is directly proportional to the phonon mean free path. Thus the introduction of dopants reduces the phonon mean free path and gives a reduced value for thermal diffusivity in doped specimens.[32] Thus, a considerable ZT value can be expected in this $Bi_2Se_{3-x}Te_x$ material.

Conclusions

In summary, $Bi_2Se_{3-x}Te_x$ nanosheets have been successfully synthesized by a "green" and facile approach in the presence of EG at a reaction temperature of 180 °C for 25 min. The electrical conductivities of the products can be tuned via changing the tellurium doping concentration. The sample with x_{Te} = 0.3 shows an increase in the electrical conductivity due to the substitution of Te atoms with Se atoms. The optimal thermo-electric transport performance is found to be the $Bi_2eS_{2.7}Te_{0.3}$ nanosheet, which exhibits values of -150 μV K^{-1} at 473 K and a power factor of 178 μW m^{-1} K^{-2} at 523 K. This work demonstrates that the $Bi_2Se_{3-x}Te_x$ nanosheets with defined morphology can be synthesized by a facile solvothermal protocol, which may be a promising approach for the development of new types of highly efficient thermoelectric materials.

Acknowledgements

References

1 R. Venkatasubramanian, E. Siivola, T. Colpitts and B. O'Quinn, Nature, 2001, **413**, 597–602.

2 S. G. Jeffrey, J. R. Lim, C. K. Huang and J. P. Fleurial, Nat. Mater., 2003, **2**, 528–531.

3 A. Saji, S. Ampili, S. H. Yang, K. J. Ku and M. Elizabeth, J. Phys.: Condens. Matter, 2005, **17**, 2873–2888.

4 T. C. Harman, P. J. Taylor, M. P. Walsh and B. E. LaForge, Science, 2002, **297**, 2229–2232.

5 K. F. Hsu, S. Loo, F. Guo, W. Chen, J. S. Dyck, C. Uher, T. Hogan, E. K. Polychroniadis and M. G. Kanatzidis, Science, 2004, **303**, 818–821.

6 D. Y. Chung, T. Hogan, P. Brazis, L. M. Rocci, C. Kannewurf, M. Bastea, C. Uher and M. G. Kanatzidis, Science, 2000, **287**, 1024–1027.

7 F. J. Disalvo, Science, 1999, **285**, 703–706.

8 H. K. Lyeo, A. A. Khajetoorians, L. Shi, K. P. Pipe, J. R. Rajeev, A. Shakouri and C. K. Shih, Science, 2004, **303**, 816–818.

9 K. Kadel, L. Kumari, W. Li, Z. Huang, J. Yu and P. P. Provencio, Nanoscale Res. Lett., 2011, **6**, 57.

10 S. Ajay, Y. Y. Zhao, L. G. Yu, K. K. A. Michael, M. S. Dresselhaus and Q. H. Xiong, Nano Lett., 2012, **12**, 1203–1209.

11 M. Scheele, N. Oeschler, I. Veremchuk, K. G. Reinsberg, A. M. Kreuziger, A. Kornowski, J. Broekaert, C. Klinke and H. Weller, ACS Nano, 2010, **4**, 4283–4291.

12 W. Xie, J. He, H. J. Kang, X. Tang, S. Zhu, M. Laver, S. Wang, J. R. D. Copley, C. M. Brown, Q. Zhang and T. M. Tritt, Nano Lett., 2010, **10**, 3283–3289.

13 Y. Zhao, J. S. Dyck, B. M. Hernandez and C. Burda, J. Phys. Chem. C, 2010, **114**, 11607–11613.

14 Y. Pei, X. Shi, A. LaLonde, H. Wang, L. Chen and G. J. Snyder, Nature, 2011, **473**, 66–69.

15 A. Majumdar, Science, 2004, **303**, 777–778.

16 A. Majumdar, Nat. Nanotechnol., 2009, **4**, 214–215.

17 Y. F. Lin, H. W. Chang, S. Y. Lu and C. W. Liu, J. Phys. Chem. C, 2007, **111**, 18538–18544.

18 Y. Xia, D. Qian, D. Hsieh, L. Wray, A. Pal, H. Lin, A. Bansil, D. Grauer, Y. S. Hor, R. J. Cava and M. Z. Hasan, Nat. Phys., 2009, **5**, 398–402.

19 L. D. Alegria, M. D. Schroer, A. Chatterjee, G. R. Poirier, M. Pretko, S. K. Patel and J. R. Petta, Nano Lett., 2012, **12**, 4711–4714.

20 D. Kong, Y. Chen, J. J. Cha, Q. Zhang, J. G. Analytis, K. Lai, Z. Liu, S. S. Hong, K. J. Koski, S. K. Mo, Z. Hussain, I. R. Fisher, Z. X. Shen and Y. Cui, Nat. Nanotechnol., 2011, **6**, 705–709.

21 L. E. Bell, Science, 2008, **321**, 1457–1461.

22 S. C. Liufu, L. D. Chen, Q. Yao and C. F. Wang, Appl. Phys. Lett., 2007, **90**, 112106.

23 Z. L. Sun, S. C. Liufu and L. D. Chen, Dalton Trans., 2010, **39**, 10883–10887.

24 Z. L. Sun, S. C. Liufu, X. H. Chen and L. D. Chen, CrystEngComm, 2010, **12**, 2672–2674.

25 Z. L. Sun, S. C. Liufu, R. H. Liu, X. H. Chen and L. D. Chen, J. Mater. Chem., 2011, **21**, 2351–2355.

26 P. Lošťák, L. Beneš, S. Civiš and H. Süssmann, J. Mater. Sci., 1990, **25**, 277–282.

27 P. Janíček, Č. Drašar, L. Beneš and P. Lošťák, Cryst. Res. Technol., 2009, **44**, 505–510.

28 J. Horak, M. Vlcek, J. Navratil, S. Hu, C. Uher, P. Lošťák, Č. Drašar and S. Karamazov, in Proceedings of the International Joint Conferences "Thermal Conductivity 25"

and "Thermal Expansion 13", Ann Arbor, Michigan, United States, June 13–16, 1999, p. 106.

29 J. Kašparová, Č. Drašar, A. Krejčová, L. Beneš, P. Lošťák, W. Chen, Z. H. Zhou and C. Uher, *J. Appl. Phys.*, 2005, **97**, 103720.

30 E. K. Shokr, E. M. M. Ibrahim, A. M. Abdel Hakeem and A. M. Adam, *J. Exp. Theor. Phys.*, 2013, **116**, 166–172.

31 A. Saji and M. Elizabeth, *Mater. Res. Bull.*, 2001, **36**, 2251–2261.

32 S. D. George, S. Augustine, E. Mathai, P. Radhakrishnan, V. P. N. Nampoori1 and C. P. G. Vallabhan, *Phys. Status Solidi A*, 2003, **196**, 384–389.

33 R. Castro, T. M. Zapata, V. R. Moo, P. B. Pérez and J. L. Pena, *J. Phys. D: Appl. Phys.*, 1999, **32**, 1194–1197.

34 J. P. Fu, S. Y. Song, X. G. Zhang, F. Cao, L. Zhou, X. Y. Li and H. J. Zhang, *CrystEngComm*, 2012, **14**, 2159–2165.

35 C. Xiao, X. M. Qin, J. Zhang, R. An, J. Xu, K. Li, B. X. Cao, J. L. Yang, B. J. Ye and Y. Xie, *J. Am. Chem. Soc.*, 2012, **134**, 18460–18466.

36 X. H. Yang, X. Wang and Z. D. Zhang, *J. Cryst. Growth*, 2005, **276**, 566–570.

37 Y. X. Zhao and C. Burda, *ACS Appl. Mater. Interfaces*, 2009, **1**, 1259–1263.

38 W. Richter, H. Köhler and C. R. Becke, *Phys. Status Solidi B*, 1977, **84**, 619.

39 K. M. F. Shahil, M. Z. Hossain, V. Goyal and A. A. Balandin, *J. Appl. Phys.*, 2012, **111**, 054305.

40 G. H. Zhang, H. J. Qin, J. Teng, J. D. Guo, Q. L. Guo, X. Dai, Z. Fang and K. H. Wu, *Appl. Phys. Lett.*, 2009, **95**, 053114.

41 S. Y. F. Zhao, C. Beekman, L. J. Sandilands, J. E. J. Bashucky, D. Kwok, N. Lee, A. D. LaForge, S. W. Cheong and K. S. Burch, *Appl. Phys. Lett.*, 2011, **98**, 141911.

42 H. M. Xu, G. Chen, R. C. Jin, J. Pei, Y. Wang and D. H. Chen, *CrystEngComm*, 2013, **15**, 1618–1625.

43 K. J. Koski, C. D. Wessells, B. W. Reed, J. J. Cha, D. S. Kong and Y. Cui, *J. Am. Chem. Soc.*, 2012, **134**, 13773–13779.

44 J. Zhang, Z. P. Peng, A. Soni, Y. Y. Zhao, Y. Xiong, B. Peng, J. B. Wang, M. S. Dresselhaus and Q. H. Xiong, *Nano Lett.*, 2011, **11**, 2407–2414.

45 D. B. Wang, D. B. Yu, M. S. Mo, X. M. Liu and Y. T. Qian, *J. Cryst. Growth*, 2003, **253**, 445–451.

46 G. Z. Shen, D. Chen, K. B. Tang and Y. T. Qian, *Nanotechnology*, 2004, **15**, 1530–1534.

47 P. F. Hu, Y. L. Cao, D. Z. Jia and L. X. Wang, *Mater. Lett.*, 2010, **64**, 493–496.

48 J. R. Wiese and L. Muldawer, *J. Phys. Chem. Solids*, 1960, **15**, 13–16.

49 J. R. Drabble and C. H. L. Goodman, *J. Phys. Chem. Solids*, 1958, **5**, 142–144.

50 T. H. Kim, J. H. Baeck, H. J. Choi, K. H. Jeong, M. H. Cho, B. C. Kim and K. T. Jeong, *J. Phys. Chem. C*, 2012, **116**, 3737–3746.

51 W. Richter, H. Köhler and C. R. Becke, *Phys. Status Solidi B*, 1977, **84**, 619.

52 A. Soni, Y. Y. Zhao, L. G. Yu, M. K. K. Aik, M. S. Dresselhaus and Q. H. Xiong, *Nano Lett.*, 2012, **12**, 1203–1209.

53 S. S. Farvid, M. Hegde and P. V. Radovanovic, *Chem. Mater.*, 2013, **25**, 233–244.

54 C. Kongmark, R. Coulter, S. Cristol, A. Rubbens, C. Pirovano, A. Lofberg, G. Sankar, W. V. Beek, E. B. Richard and R. N. Vannier, *Cryst. Growth Des.*, 2012, **12**, 5994–6003.

55 F. Ye, T. Mori, D. R. Ou, J. Zou and J. Drennan, *Solid State Ionics*, 2009, **180**, 1414–1420.

56 I. Rusakova, T. O. Ely, C. Hofmann, D. P. Centurión, C. S. Levin, N. J. Halas, A. Lüttge and K. H. Whitmire, *Chem. Mater.*, 2007, **19**, 1369–1375.

57 A. Soni, Y. Y. Zhao, L. G. Yu, M. K. K. Aik, M. S. Dresselhaus and Q. H. Xiong, *Nano Lett.*, 2012, **12**, 1203–1209.

58 Z. M. He, C. Stiewe, D. Platzek, G. Karpinski, E. Müller, S. H. Li, M. Toprak and M. Muhammed, *J. Appl. Phys.*, 2007, **101**, 053713.

59 M. K. Han, K. Ahn, H. J. Kim, J. S. Rhyee and S. J. Kim, *J. Mater. Chem.*, 2011, **21**, 11365–11370.

60 M. K. Han, K. Hoang, H. J. Kong, R. Pcionek, C. Uher, K. M. Paraskevopoulos, S. D. Mahanti and M. G. Kanatzidis, *Chem. Mater.*, 2008, **20**, 3512–3520.

61 G. Joshi, H. Lee, Y. C. Lan, X. W. Wang, G. H. Zhu, D. Z. Wang, R. W. Gould, D. C. Cuff, M. Y. Tang, M. S. Dresselhaus, G. Chen and Z. F. Ren, *Nano Lett.*, 2008, **8**, 4670–4674.

62 R. C. Jin, G. Chen, J. Pei and C. S. Yan, *New J. Chem.*, 2012, **36**, 2574–2579.

63 D. M. Rowe, *Thermoelectrics Handbook: Macro to Nano*, CRC Press, Boca Raton, London, New York, 2006.

64 R. C. Jin, G. Chen, J. Pei, J. X. Sun and Q. Wang, *CrystEngComm*, 2012, **14**, 4461–4466.